RESEARCH ARTICLE

Resting-state network complexity and magnitude changes in neonates with severe hypoxic ischemic encephalopathy

Hong-Xin Li[1], Min Yu[2], Ai-Bin Zheng[3], Qin-Fen Zhang[1], Guo-Wei Hua[1], Wen-Juan Tu[1], Li-Chi Zhang[4, 5, *]

1 Department of Neonatology, Changzhou Children's Hospital, Changzhou, Jiangsu Province, China
2 Graduate Student, Nantong University, Nantong, Jiangsu Province, China
3 Department of Children's Health Research Center, Changzhou Children's Hospital, Changzhou, Jiangsu Province, China
4 Institute for Medical Imaging Technology, School of Biomedical Engineering, Shanghai Jiao Tong University, Shanghai, China
5 Department of Radiology and BRIC, University of North Carolina at Chapel Hill, Chapel Hill, NC, USA

Funding: *This study was supported by the Jiangsu Maternal and Child Health Research Project of China, No. F201612 (to HXL); the Changzhou Science and Technology Support Plan of China, No. CE20165027 (to HXL); the Changzhou City Planning Commission Major Science and Technology Projects of China, No. ZD201515 (to HXL); the Changzhou High Level Training Fund for Health Professionals of China, No. 2016CZBJ028 (to HXL).*

Graphical Abstract

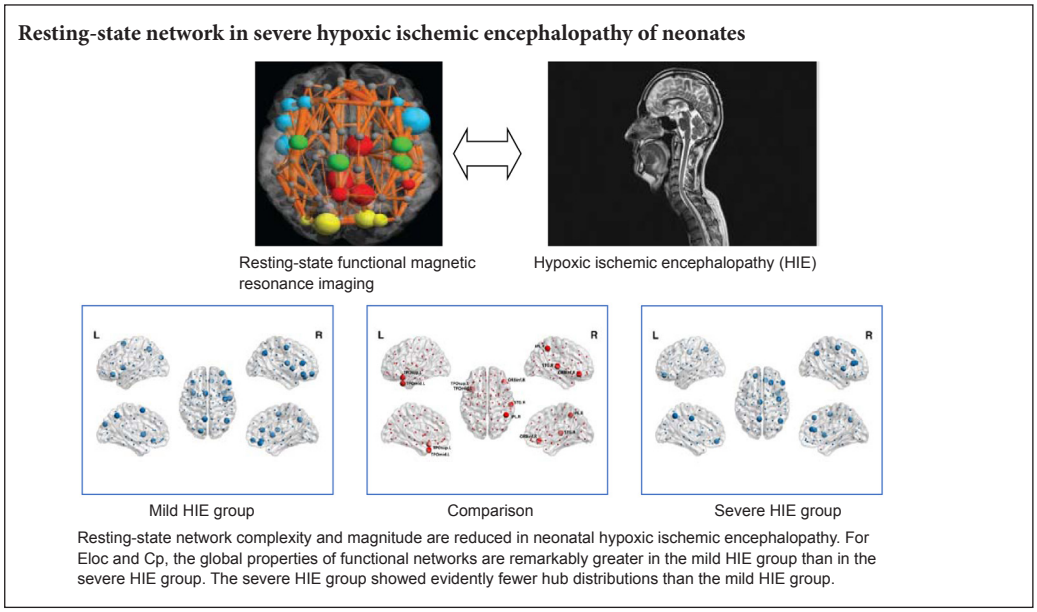

Correspondence to:
Li-Chi Zhang, MD,
lichizhang@sjtu.edu.cn.

orcid:
0000-0003-4396-4566
(Li-Chi Zhang)

doi: *10.4103/1673-5374.247468*

Received: *April 14, 2018*
Accepted: *August 31, 2018*

Abstract

Resting-state functional magnetic resonance imaging has revealed disrupted brain network connectivity in adults and teenagers with cerebral palsy. However, the specific brain networks implicated in neonatal cases remain poorly understood. In this study, we recruited 14 term-born infants with mild hypoxic ischemic encephalopathy and 14 term-born infants with severe hypoxic ischemic encephalopathy from Changzhou Children's Hospital, China. Resting-state functional magnetic resonance imaging data showed efficient small-world organization in whole-brain networks in both the mild and severe hypoxic ischemic encephalopathy groups. However, compared with the mild hypoxic ischemic encephalopathy group, the severe hypoxic ischemic encephalopathy group exhibited decreased local efficiency and a low clustering coefficient. The distribution of hub regions in the functional networks had fewer nodes in the severe hypoxic ischemic encephalopathy group compared with the mild hypoxic ischemic encephalopathy group. Moreover, nodal efficiency was reduced in the left rolandic operculum, left supramarginal gyrus, bilateral superior temporal gyrus, and right middle temporal gyrus. These results suggest that the topological structure of the resting state functional network in children with severe hypoxic ischemic encephalopathy is clearly distinct from that in children with mild hypoxic ischemic encephalopathy, and may be associated with impaired language, motion, and cognition. These data indicate that it may be possible to make early predictions regarding brain development in children with severe hypoxic ischemic encephalopathy, enabling early interventions targeting brain function. This study was approved by the Regional Ethics Review Boards of the Changzhou Children's Hospital (approval No. 2013-001) on January 31, 2013. Informed consent was obtained from the family members of the children. The trial was registered with the Chinese Clinical Trial Registry (registration number: ChiCTR1800016409) and the protocol version is 1.0.

Key Words: *nerve regeneration; neonates; hypoxic ischemic encephalopathy; resting-state functional magnetic resonance imaging; brain networks; small-world organization; brain functional connectivity; local efficiency; clustering coefficient; neural regeneration*

Chinese Library Classification No. *R445; R722*

Introduction

Magnetic resonance imaging (MRI) has had a dramatic impact on neuroscience and clinical research, as it enables noninvasive observation of *in-vivo* anatomical structures and functional connectivity of the brain. Related techniques have also played a central role in neonatal brain development research. For example, functional MRI (fMRI) enables measurement of the blood oxygen level-dependent time series of hemodynamic changes in the brain (Gore, 2003; Fox and Greicius, 2010). fMRI is increasingly showing potential in early diagnoses, prevention, and medication evaluation in several "connection offset" brain mental disorders (such as Alzheimer's disease, epilepsy, and schizophrenia) (Liao et al., 2012; Kang and Sperling, 2017). At present, the topological relationships between the nodes and edges of complex networks are widely studied in the biomedical field. Such research may center around explorations of brain structure, function, and network utility (Zhang et al., 2016, 2017a, 2017b). Brain functional networks can be used to describe the correlations among the nodes of the cerebral cortex in space. These are generally viewed as undirected networks. Watts and Strogatz (1998) found many real networks to have small-world network characteristics. Resting-state fMRI (rs-fMRI) involves the collection of fMRI data in a task-free state, and is usually applied to examine correlated activity patterns or functional connectivity among different gray matter brain regions (Biswal et al., 1995). Many studies have investigated the functional networks of the neonatal brain using rs-fMRI. For instance, Fransson et al. (2011) characterized five resting-state cerebral networks in unsedated infants born at full term. Normal term infants appear to have small-world networks with effective and economic structures (De Asis-Cruz et al., 2015). Smyser et al. (2016) found that resting state network complexity and scope were reduced in premature infants compared with full-term infants.

Neonates with severe hypoxic ischemic encephalopathy (HIE) have a higher rate of poor development and physical or cognitive deficits compared with those with mild HIE (Kurinczuk et al., 2010; Lemmon et al., 2017; Li et al., 2017). However, functional connectivity in neonatal patients with HIE has not been characterized. fMRI has high time and spatial resolution, which can increase the accuracy of prognosis. Fransson et al. (2011) used rs-fMRI to find that the default network in full-term newborns mainly involves basic brain regions, such as the motor area, sensory area, auditory area, and visual area. However, in adults, the brain regions comprising the default network include the posterior cingulate gyrus, medial prefrontal cortex, dorsal region of the thalamus, cuneus and precuneus, hippocampus, and partial temporal lobe.

The development of the central network is a gradual process of reorganization that takes place from birth to adulthood. De Asis-Cruz et al. (2015) found that the neonatal brain network already has the connection characteristics of a small-world network. This indicates that there is an optimal balance between functional brain integration and segregation that is critical for efficient transfer of local and global information. Neonates have a cost-efficient brain functional network, where global and local efficiencies are greater than the network cost (De Asis-Cruz et al., 2015). The neonate small-world network is economical as well (De Asis-Cruz et al., 2015). Although some studies have reported that brain injury can lead to abnormal whole-brain structural connectivity (Ballester-Plané et al., 2017), few studies have examined HIE-related alternations of functional connectivity in neonatal brain networks. Thus, in this study, we used rs-fMRI to examine global and local brain functional network properties in infants with mild *vs*. severe HIE.

Participants and Methods

Participants

This prospective cohort study was performed at the Changzhou Children's Hospital of China. The study protocol was approved by the Regional Ethics Review Boards of Changzhou Children's Hospital (approval No. 2013-001) (**Additional file 1**) on January 31, 2013. Parental informed consent (**Additional file 2**) was obtained for each participant prior to participation in the study. The trial was registered with the Chinese Clinical Trial Registry (registration number: ChiCTR1800016409) on May 31, 2018, and the protocol version is 1.0.

From January 2013 to December 2015, we recruited 28 full-term neonates with HIE (14 mild cases and 14 severe cases). Diagnosis and inclusion criteria were in accordance with the HIE diagnostic criteria and clinical classification of practical neonatal HIE, revised by the Neonatology Group of the Chinese Pediatric Society of the Chinese Medical Association in Changsha (Leandrou et al., 2016). MRI data were only acquired for neonates aged 8–14 days, as they were deemed sufficiently clinically stable to undergo MRI. Neonatal patients with any of the following were excluded from the study: genetic metabolic diseases, central nervous system infection, congenital malformation of the brain, and chromosomal abnormality. **Table 1** presents the demographic information and clinical characteristics of all the participants. There were no significant differences in sex, gestational age, mean weight, or age on the day of examination between the two groups ($P > 0.05$). **Figure 1** contains a flow chart of the study procedure. The writing and editing of this article were performed in accordance with the STrengthening the Reporting of OBservational Studies in Epidemiology (STROBE) Statement (**Additional file 3**).

Image acquisition

Imaging was performed using a 3T Philips Achieva MRI scanner (Philips, Rotterdam, the Netherlands) located in the Changzhou Children's Hospital of China. All infants were imaged during natural sleep. Heart and respiratory rates were automatically and continuously monitored by the scanner. A NICU staff member and one family member of the participant were continuously present in the scanner room throughout the study. We previously developed an infant insulation cap for magnetic resonance examination (patent No. ZL 2017 2 0026347.2) that can provide adequate hearing protection for children. The imaging parameters are sum-

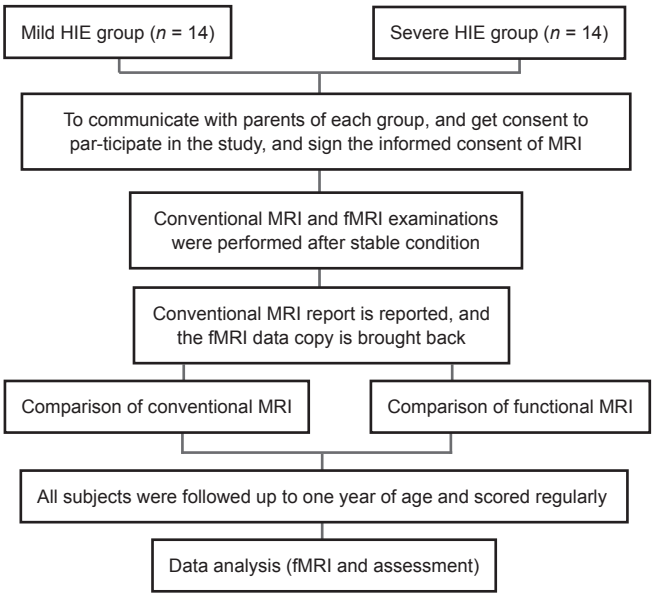

Figure 1 Flow chart of the study procedure.
HIE: Hypoxic ischemic encephalopathy; MRI: magnetic resonance imaging; fMRI: functional magnetic resonance imaging.

marized as follows: For T1w, repetition time = 9.3 ms, echo time = 4.4 ms, image matrix = 180 × 180 mm^2, voxel size = 0.56 × 0.56 × 0.6 mm^3, slice thickness = 0.6 mm, number of slices = 200, scan time = 8 minutes 19 seconds; For rs-fMRI, repetition time = 1500 ms, echo time = 27 ms, image matrix = 168 × 168 mm^2, voxel size = 2.4 × 2.4 × 3 mm^3, number of slices = 30, flip angle = 80°, volume number = 210, scan time = 5 minutes 19 seconds. The total duration of the scanning session was 13 minutes 38 seconds.

Data preprocessing

For data preprocessing of the T1w images, we conducted ITK-based N3 bias correction and used a histogram-matching program for overall intensity normalization, as described in Coupé et al. (2011). For the fMRI images, preprocessing is summarized as follows: We commenced by removing the first five frames for magnetization equilibrium, and then used SPM8 (https://www.fil.ion.ucl.ac.uk/spm/soft-ware/spm8/), REST (http://www.restfmri.net/forum/REST_V1.8), and DPARSFA (http://rfmri.org/DPARSF) to reduce the effects of nuisance signals. We used the rigid-body transformation for head motion correction, and images with head motion larger than 2 mm or 2° were discarded. We then performed the spatial smoothing procedure with the FWHM filter as 6 × 6 × 6 in voxels for denoising. Band-pass filters ($0.01 \leq f \leq 0.1$ Hz) were applied to avoid physiological noise and measurement errors. Head motion parameters (Friston24) (Yan et al., 2013) were regressed out from the rs-fMRI data. Note that we did not conduct spatial registration for the rs-fMRI data. The subsequent analysis was performed in the participant native space to prevent potential registration error that might affect the evaluation results. Statistical analysis was performed using SPSS version 22 (IBM, Armonk, NY, USA). Group comparisons of Fisher's z-transformed correlation coefficients (z(r)) were conducted using two-sample, two-tailed *t*-tests. And baseline data were analyzed by student's *t*-test.

Network construction

As our goal was to investigate functional connectivity in different brain regions, it was necessary to obtain prerequisite whole-brain labeling information. Conventional studies have implemented non-rigid registration of obtained rs-fMRI data to the Montreal Neurosciences Institute atlas template and used its corresponding label map for subsequent network construction works (Striem-Amit et al., 2011). However, the Montreal Neurosciences Institute atlas template was designed for the adult brain, which differs greatly from the neonatal brain. Thus, this tool is inappropriate for the present study. We adopted the University of North Carolina infant 0-1-2 atlases (https://www.med.unc.edu/bric/ideagroup/free-softwares/unc-infant-0-1-2-atlases) as replacements for the Montreal Neurosciences Institute atlas. This has been done for similar research (Shi et al., 2011). The University of North Carolina infant 0-1-2 atlases were constructed from MRI scans from 95 normal infants (56 males and 39 females) using state-of-the-art infant MR segmentation and groupwise registration methods. It includes three atlases: one each for neonate, 1-year-old, and 2-year-old cases. Each atlas comprises a set of three-dimensional images including an intensity model, tissue probability maps, and anatomical parcellation map (*i.e.*, automated anatomical labeling map).

We used the neonate images from the University of North Carolina infant 0-1-2 atlases to label our rs-fMRI images with the aid of the corresponding T1w structural MRI data. Specifically, we first used the SPM8 software to co-register the T1w images to the mean-echo planar image from the fMRI data. The cost function was set as the Entropy Correlation Coefficient. Then, we performed non-rigid registration of the neonate atlas to the aligned T1w image using the antsRegistration program (https://github.com/ANTsX/ANTs), and warped the automated anatomical labeling map to the native space of the fMRI data.

The network construction based on the obtained labeling information is given as follows: For each region-of-interest detected *via* automated anatomical labeling (**Table 2**) in the rs-fMRI data, the blood oxygen level-dependent signals were averaged together to make an overall blood oxygen level-dependent time series representing that specific region-of-interest. We then constructed correlation matrices by computing Pearson's correlation coefficients for each automated anatomical labeling region-of-interest pair. The degree centrality-based hubs or degree hubs were defined as nodes with degree ≥ mean degree ± 1 SD. We also employed Fransson's method for calculating networks associated with hubs (Fransson et al., 2011). Specifically, networks associated with each candidate hub were assessed by computing statistical parametrical maps at the individual level, and a subsequent *t*-test was performed at the second level ($P < 0.005$) for each cortical hub candidate. The small world index (σ) is a scalar value that quantifies the 'small-world-ness' of a

network (Humphries and Gurney, 2008); $\sigma > 1$, where $\sigma = \gamma/\lambda$ ($\gamma = Cp/C_{rand}$, $\lambda = Lp/L_{rand}$) indicates a small world network (Watts and Strogatz, 1998). Local efficiency was calculated as $(E_{loc}) = E_{local} = \sum i\varepsilon V E(i)$ and nodal efficiency was calculated as $(E_{nodal}) = \frac{1}{N(N-1)}\sum_{i,j\varepsilon V, i\neq j}\frac{1}{lij}$.

Neurodevelopmental test

A neurodevelopmental test called the Child Development Center of China test (CDCC) was performed for all participants at one year of age. The CDCC test contains a mental development index and a psychomotor development index. A mental development or psychomotor development index score of < 85 indicates an abnormality (Fan, 1989).

Results

There were no significant differences in age, sex, gestational age, and weight between the mild and severe HIE groups ($P > 0.05$). Patients with severe HIE showed a significantly higher rate of abnormal CDCC scores. Patients in the severe HIE group were also more likely to have abnormal psychomotor or mental development index scores compared with those in the mild HIE group ($P < 0.05$; **Table 1**).

Altered global properties of functional networks in HIE patients

The two patient groups showed small-world organization of functional networks, characterized by $\gamma > 1$ and $\lambda \approx 1$ (**Figure 2**). However, compared with the mild HIE group, those in the severe HIE group exhibited decreased E_{loc} in the functional networks over a wide range of thresholds ($P = 0.0288$). Additionally, we found a low clustering coefficient (Cp) in the severe HIE group ($P = 0.0346$, *vs*. mild HIE group) (**Table 3**). There were no significant differences between groups in terms of the other network metrics (**Table 3**).

Altered regional properties of functional networks in HIE patients

We first identified the hub regions of the functional networks for each group. The nodes were considered brain hubs if their nodal efficiencies were at least 1 SD greater than the average nodal efficiency of the network. We found significantly fewer hub distributions in the severe HIE group (8 hubs) compared with the mild HIE groups (14 hubs) (**Figure 3A** and **B**, and **Table 4**). Further statistical analysis revealed that patients with severe HIE had reduced nodal efficiency in the left rolandic operculum, left supramarginal gyrus, left and right temporal pole (superior temporal gyrus), and right temporal pole (middle temporal gyrus) (**Figure 3C** and **Table 5**).

Table 1 Comparison of mild and severe patients in terms of age at MRI, sex, gestational age, and birth weight

Item	Mild HIE (n = 14)	Severe HIE (n = 14)	t/x^2	P
Gestational age (week)	40.3±2.8	39.1±2.9	1.224	> 0.05
Birth weight (g)	3367±480	3167±340	1.001	> 0.05
Age at MRI (days)	16.3±4.4	14.3±4.9	1.142	> 0.05
Sex (male/female)	7/5	9/5	0.104	> 0.05
MDI	96.6±23.7	64.6±13.7	1.965	< 0.05
PDI	90.5±33.1	72.5±23.9	1.812	< 0.05

Data are expressed as the mean ± SD (Student's t-test), except the sex ratio. HIE: Hypoxic ischemic encephalopathy; MRI: magnetic resonance imaging; MDI: mental development index; PDI: psychomotor development index.

Table 2 Cortical and subcortical regions of interest defined in the study

Index	Regions	Abbreviations
1,2	Precental gyrus	PreCG
3,4	Superior frontal gyrus, dorsolateral	SFGdor
5,6	Superior frontal gyrus, orbital part	ORBsup
7,8	Middle frontal gyrus	MFG
9,10	Middle frontal gyrus, orbital part	ORBmid
11,12	Inferior frontal gyrus, opercular part	IFGoperc
13,14	Inferior frontal gyrus, triangular part	IFGtriang
15,16	Inferior frontal gyrus, orbital part	ORBinf
17,18	Rolandic operculum	ROL
19,20	Supplementary motor area	SMA
21,22	Olfactory cortex	OLF
23,24	Superior frontal gyrus, medial	SFGmed
25,26	Superior frontal gyrus, medial orbital	ORBsupmed
27,28	Gyrus rectus	REC
29,30	Insula	INS
31,32	Anterior cingulate and paracingulate gyri	ACG
33,34	Median cingulate and paracingulate gyri	DCG
35,36	Posterior cingulate gyrus	PCG
37,38	Hippocampus	HIP
39,40	Parahippocampal gyrus	PHG
41,42	Amygdala	AMYG
43,44	Calcarine fissure and surrounding cortex	CAL
45,46	Cuneus	CUN
47,48	Lingual gyrus	LING
49,50	Superior occipital gyrus	SOG
51,52	Middle occipital gyrus	MOG
53,54	Inferior occipital gyrus	IOG
55,56	Fusiform gyrus	FFG
57,58	Postcentral gyrus	PoCG
59,60	Superior parietal gyrus	SPG
61,62	Inferior parietal, supramarginal and angular gyri	IPL
63,64	Supramarginal gyrus	SMG
65,66	Angular gyrus	ANG
67,68	Precuneus	PCUN
69,70	Paracentral lobule	PCL
71,72	Caudate nucleus	CAU
73,74	Lenticular nucleus, putamen	PUT
75,76	Lenticular nucleus, pallidum	PAL
77,78	Thalamus	THA
79,80	Heschl gyrus	HES
81,82	Superior temporal gyrus	STG
83,84	Temporal pole: superior temporal gyrus	TPOsup
85,86	Middle temporal gyrus	MTG
87,88	Temporal pole: middle temporal gyrus	TPOmid
89,90	Inferior temporal gyrus	ITG

Discussion

Neonatal HIE caused by perinatal hypoxia craniocerebral injury is the main cause of neonatal death. At present, the

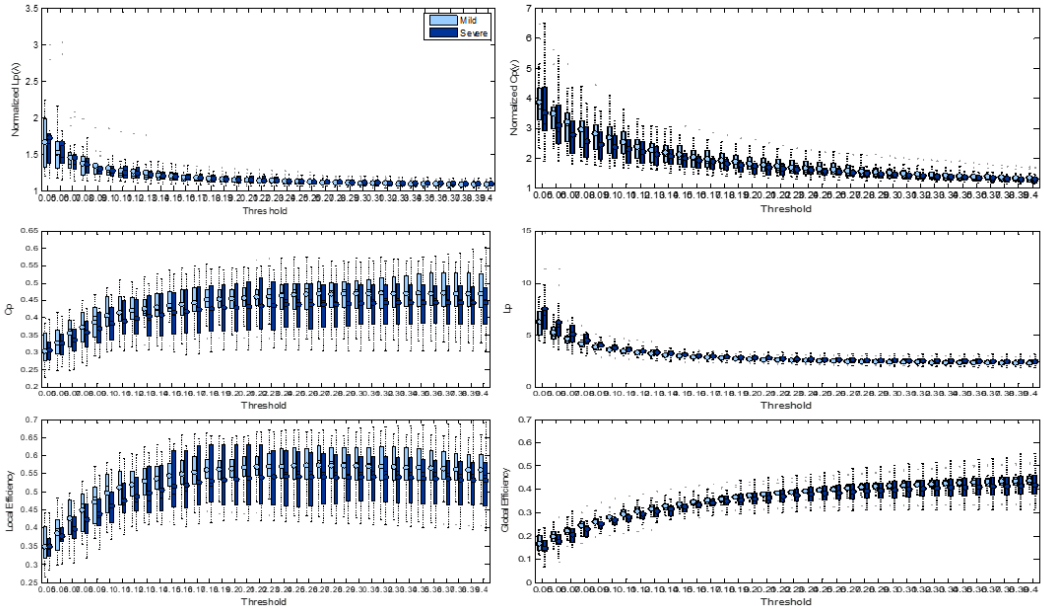

Figure 2 Topological properties of functional networks in mild *vs.* severe HIE groups.
The light blue color represents the mild HIE group and the dark blue represents the severe HIE group. For normalized L_p and normalized C_p, $\gamma > 1$ and $\lambda \approx 1$. For E_{loc} and C_p, all thresholds were significantly greater in the mild HIE group compared with the severe HIE group ($P < 0.05$). Data are expressed as the mean ± SD (two-sample *t*-test). HIE: Hypoxic ischemic encephalopathy.

Table 3 Area under the curve values of global network properties in the mild *vs.* severe HIE groups

Item	Mild HIE (n = 14)	Severe HIE (n = 14)	t	P
Network strength (S_p)	0.4172±0.0134	0.4061±0.0152	1.118	> 0.05
Global efficiency (E_{glob})	0.1371±0.0096	0.1266±0.0136	1.126	> 0.05
Local efficiency (E_{loc})	0.1879±0.0369	0.1631±0.0234	1.852	< 0.05
Path length (L_p)	1.0341±0.0824	1.0937±0.1148	–1.326	> 0.05
Clustering coefficient (C_p)	0.1669±0.0304	0.1361±0.0273	1.798	< 0.05
γ	183.34±4.04	184.56±7.04	–1.086	> 0.05
λ	23.74±0.56	29.52±0.67	–1.897	< 0.05

Data are expressed as the mean ± SD (two-sample *t*-test). HIE: Hypoxic ischemic encephalopathy.

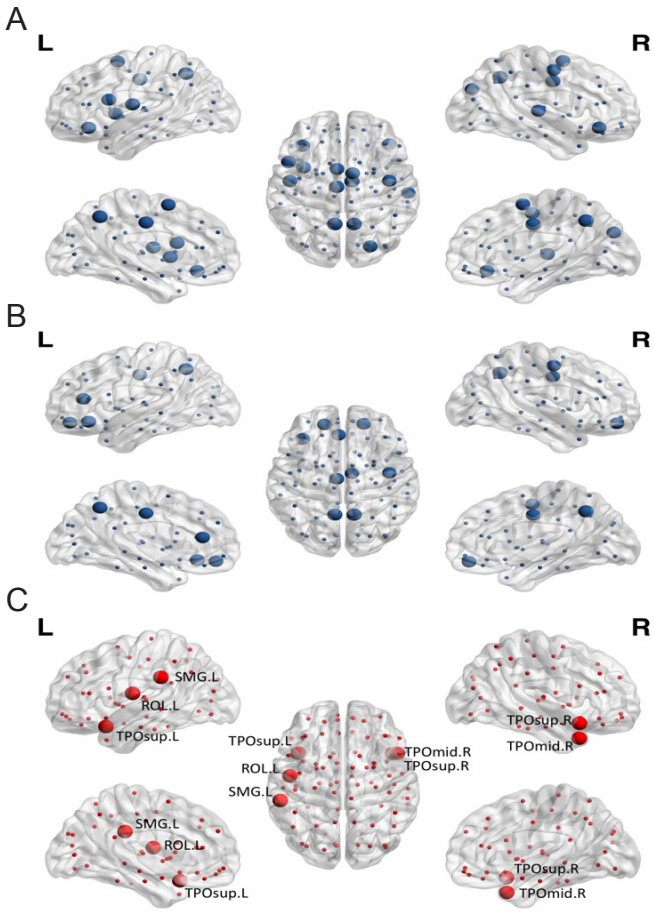

Figure 3 Distribution of hub regions in the functional structural networks of mild and severe HIE patients, nodes with decreased efficiency in severe HIE patients.
(A, B) Three-dimensional representation of hub distributions in the mild (A) and severe (B) HIE groups. The hub nodes are shown in blue with node sizes, indicating their nodal efficiency values. (C) The disrupted nodes in severe patients are shown in red with node sizes, indicating the significance of between-group differences in regional efficiency. Data visualized using BrainNet Viewer software (http://www.nitrc.org/projects/bnv/). HIE: Hypoxic ischemic encephalopathy.

incidence rate in China is about 6/1000 (Krishnan and Shroff, 2016). Neonatal HIE is not only a serious threat to neonatal life, but also one of the most common causes of post-neonatal disability (Liu et al., 2012). It can lead to cerebral palsy, delayed neurodevelopment, visual impairment, hearing impairment, and serious neurological abnormalities associated with cognitive defects, especially in children with severe HIE (Huang and Castillo, 2008; Krishnan and Shroff, 2016; Du et al., 2018). Although neural imaging techniques such as cerebral CT, ultrasound, and MRI have facilitated the diagnosis of brain injury, the sensitivity and specificity regarding damage of functional areas is poor, hindering prognosis (Coleman et al., 2013; Jose et al., 2013; Duong and Watts, 2016). We attempted to address this in the present study by choosing to use rs-fMRI to collect brain functional connectivity data in infants with mild vs. severe HIE, and using these data to explore differences in the global and local brain functional network properties.

We compared brain global and regional network properties using probabilistic imaging and graph theoretic methods. We analyzed global brain networks by calculating

Table 4 Hub regions of functional networks in mild and severe HIE patients

Hub	Distribution	E_{nodal}/Mean
Mild HIE group		
Pre CG.R	Right frontal	1.072677922
IFG operc.L	Left frontal	1.088102615
ORB inf.L	Left frontal	1.115541314
ORB inf.R	Right frontal	1.078078658
ROL.L	Left insular	1.096984028
SMA.L	Left frontal	1.079337018
SMA.R	Right frontal	1.08210704
INS.L	Left insular	1.086697346
DCG.L	Left limbic	1.115137309
DCG.R	Right limbic	1.115109549
SOG.R	Right occipital	1.070131958
PCUN.L	Left parietal	1.173990756
PCUN.R	Right parietal	1.160583338
STG.R	Right temporal	1.074150518
Severe HIE group		
ORB sup.L	Left frontal	1.111960402
ORB sup.R	Right frontal	1.099452482
ORB inf.L	Left frontal	1.139021442
ACG.L	Left limbic	1.113434026
DCG.L	Left limbic	1.106834279
DCG.R	Right limbic	1.086094592
PCUN.L	Left parietal	1.151491983
PCUN.R	Right parietal	1.193701474

HIE: Hypoxic ischemic encephalopathy.

Table 5 Hub regions with significant effects on nodal efficiency (E_{nodal}) in mild and severe patients

		E_{nodal}		
Hub	Distribution	Mild HIE group	Severe HIE group	*P* value
ROL.L	Left insular	0.4801±0.0762	0.4089±0.0865	0.032730584
SMG.L	Left parietal	0.4465±0.0898	0.3377±0.1223	0.014816123
TPO sup.L	Left temporal	0.4655±0.0812	0.3842±0.0898	0.021173549
TPO sup.R	Right temporal	0.4640±0.0690	0.3508±0.1295	0.009673193
TPO mid.R	Right temporal	0.4271±0.0636	0.3564±0.0843	0.021887484

Data are expressed as the mean ± SD (two-sample *t*-test).

the Cp and the shortest path length (Lp) to obtain two indicators (γ and λ), which can be used to determine whether there is a small-world property. If γ ≥ 1, the network is considered to have a small-world property. At birth, brain networks in babies have small-world properties (De Asis-Cruz et al., 2015). A previous study indicated that both mild and severe HIE patients have small-world properties, which is consistent with many other reports (Supekar et al., 2009). Small-world networks may be less sensitive to diseases and developmental abnormalities compared with larger networks (De Vico Fallani et al., 2017; Vecchio et al., 2017; Wang et al., 2017). This may be related to the finding that brain networks in children with attention deficit/hyperactivity disorder have small-world properties (Cao et al., 2013). In the present study, we also found that local efficiency (E_{loc}) and the clustering coefficient (C_p) were substantially lower in the severe HIE group compared with the mild HIE group, suggesting that the brain function network in the severe HIE group was underdeveloped. Healthy human brain development is mainly assessed on the basis of local node efficiency (Dosenbach et al., 2010). Regional brain network analysis is conducted by calculating the node efficiency. We found that the number of hub nodes in the severe HIE group was significantly lower than that in the mild HIE group (14 in the mild HIE group and 9 in severe HIE group). Fujii et al. (2016) reported that the left superior gyrus was strongly associated with hand coordination control ability. Króliczak et al. (2016) found that the left insular operculum is strongly associated with language development. Dupont (2002) verified that the temporal lobe is closely implicated in human memory function. Therefore, our results may in some part explain why children with severe HIE show poor hand coordination, memory, language, and cognitive function. Our CDCC test results indicate that children with severe HIE have poor hand coordination and delayed language development. These findings may be explained by dysfunction in the five disrupted nodes, including the left rolandic operculum, left supramarginal gyrus, left and right temporal pole (superior temporal gyrus), and right temporal pole (middle temporal gyrus).

This study has several limitations, including a small sample, a lack of normal control groups, and a single research method. However, the present study revealed differences in resting state network topological properties between the mild and severe HIE patients, and these data may be applicable to other forms of brain injury in children.

Resting-state network complexity and magnitude are reduced in neonatal hypoxic ischemic encephalopathy. For E_{loc} and C_p, the global properties of functional networks were significantly greater in the mild HIE group compared with the severe HIE group. The severe HIE group had a significantly smaller hub distribution compared with the mild HIE group. This study may contribute to the development of strategies for early assessment of brain development in children with severe HIE, as well as early interventions that address brain function.

Author contributions: *Definition of intellectual content of this topic and paper review: LCZ; literature search and study design: HXL; paper preparation and editing: ABZ; data acquisition: HXL, ABZ, MY and WJT; data analysis: HXL, QFZ and LCZ; statistical analysis: MY and GWH. All authors approved the final version of the paper.*
Conflicts of interest: *None declared.*
Financial support: *This study was supported by the Jiangsu Maternal and Child Health Research Project of China, No. F201612 (to HXL); the Changzhou Science and Technology Support Plan of China, No. CE20165027 (to HXL); the Changzhou City Planning Commission Major Science and Technology Projects of China, No. ZD201515 (to HXL); the Changzhou High Level Training Fund for Health Professionals of China, No. 2016CZBJ028 (to HXL). The funders did not participate in data collection and analysis, article writing or submission.*
Institutional review board statement: *The study was approved by the Regional Ethics Review Boards of the Changzhou Children's Hospital, China (approval No. 2013-001) in January, 2013. The trial was performed in accordance with the Declaration of Helsinki and relevant hospital's ethical principles. The trial was registered with the Chinese Clinical Trial Registry (registration number: ChiCTR1800016409) on May 31, 2018.*
Declaration of patient consent: *The authors certify that they have obtained all appropriate legal guardian consent forms. In the form, the legal guardians have given their consent for the patients' images and other clinical information to be reported in the journal. The patients' legal guardians understand that the patients' names and initials will not be published and due efforts will*

be made to conceal their identity.

Reporting statement: *The writing and editing of the article followed the STrengthening the Reporting of OBservational Studies in Epidemiology (STROBE) Statement.*

Biostatistics statement: *The statistical methods of this study were reviewed by the biostatistician of Changzhou Children's Hospital, China.*

Data sharing statement: *Individual participant data that underlie the results reported in this article after deidentification (text, tables, figures, and appendices) will be shared. Study protocol, informed consent form and clinical study report will be promulgated within 3 months after the completion of the trial. Results will be disseminated through presentations at scientific meetings and/or by publication in a peer-reviewed journal. Anonymized trial data will be available indefinitely at www.czetyy.com.*

Plagiarism check: *Checked twice by iThenticate.*

Peer review: *Externally peer reviewed.*

Additional files:

Additional file 1: *Ethical approval documentation (Chinese).*

Additional file 2: *Parental informed consent (Chinese).*

Additional file 3: *STROBE check list.*

References

Ballester-Plané J, Schmidt R, Laporta-Hoyos O, Junqué C, Vázquez É, Delgado I, Zubiaurre-Elorza L, Macaya A, Póo P, Toro E, de Reus MA, van den Heuvel MP, Pueyo R (2017) Whole-brain structural connectivity in dyskinetic cerebral palsy and its association with motor and cognitive function. Hum Brain Mapp 38:4594-4612.

Biswal B, Yetkin FZ, Haughton VM, Hyde JS (1995) Functional connectivity in the motor cortex of resting human brain using echo-planar MRI. Magn Reson Med 34:537-541.

Cao Q, Shu N, An L, Wang P, Sun L, Xia MR, Wang JH, Gong GL, Zang YF, Wang YF, He Y (2013) Probabilistic diffusion tractography and graph theory analysis reveal abnormal white matter structural connectivity networks in drug-naive boys with attention deficit/hyperactivity disorder. J Neurosci 33:10676-10687.

Coleman MB, Glass P, Brown J, Kadom N, Tsuchida T, Scafidi J, Chang T, Vezina G, Massaro AN (2013) Neonatal neurobehavioral abnormalities and MRI brain injury in encephalopathic newborns treated with hypothermia. Early Hum Dev 89:733-737.

Coupé P, Manjón JV, Fonov V, Pruessner J, Robles M, Collins DL (2011) Patch-based segmentation using expert priors: application to hippocampus and ventricle segmentation. Neuroimage 54:940-954.

De Asis-Cruz J, Bouyssi-Kobar M, Evangelou I, Vezina G, Limperopoulos C (2015) Functional properties of resting state networks in healthy full-term newborns. Sci Rep 5:17755.

De Vico Fallani F, Latora V, Chavez M (2017) A topological criterion for filtering information in complex brain networks. PLoS Comput Biol 13:e1005305.

Dosenbach NU, Nardos B, Cohen AL, Fair DA, Power JD, Church JA, Nelson SM, Wig GS, Vogel AC, Lessov-Schlaggar CN, Barnes KA, Dubis JW, Feczko E, Coalson RS, Pruett JR, Jr., Barch DM, Petersen SE, Schlaggar BL (2010) Prediction of individual brain maturity using fMRI. Science 329:1358-1361.

Du L, Shan L, Yue XJ, Li HH, Jia FY (2018) Does early injection of mouse nerve growth factor affect motor and cognitive abilities in high-risk infants? study protocol for a randomized parallel-controlled trial. Asia Pac J Clin Trials Nerv Syst Dis 3:74-80.

Duong TQ, Watts LT (2016) A brief report on MRI investigation of experimental traumatic brain injury. Neural Regen Res 11:15-17.

Dupont S (2002) Investigating temporal pole function by functional imaging. Epileptic Disord 4 Suppl 1:S17-22.

Fan CR (1989) CDCC Development of infant intelligence development checklist. Xin Li Xue Bao 2:130-133.

Fransson P, Aden U, Blennow M, Lagercrantz H (2011) The functional architecture of the infant brain as revealed by resting-state fMRI. Cereb Cortex 21:145-154.

Fox MD, Greicius M (2010) Clinical applications of resting state functional connectivity. Front Syst Neurosci 4:19.

Fransson P, Aden U, Blennow M, Lagercrantz H (2011) The functional architecture of the infant brain as revealed by resting-state fMRI. Cereb Cortex 21:145-154.

Fujii M, Maesawa S, Ishiai S, Iwami K, Futamura M, Saito K (2016) Neural basis of language: an overview of an evolving model. Neurol Med Chir (Tokyo) 56:379-386.

Gore JC (2003) Principles and practice of functional MRI of the human brain. J Clin Invest 112:4-9.

Huang BY, Castillo M (2008) Hypoxic-ischemic brain injury: imaging findings from birth to adulthood. Radiographics 28:417-439; quiz 617.

Humphries MD, Gurney K (2008) Network 'small-world-ness': a quantitative method for determining canonical network equivalence. PLoS One 3:e0002051.

Jose A, Matthai J, Paul S (2013) Correlation of EEG, CT, and MRI brain with neurological outcome at 12 months in term newborns with hypoxic ischemic encephalopathy. J Clin Neonatol 2:125-130.

Kang JY, Sperling MR (2017) Magnetic resonance imaging-guided laser interstitial thermal therapy for treatment of drug-resistant epilepsy. Neurotherapeutics 14:176-181.

Króliczak G, Piper BJ, Frey SH (2016) Specialization of the left supramarginal gyrus for hand-independent praxis representation is not related to hand dominance. Neuropsychologia 93:501-512.

Krishnan P, Shroff M (2016) Neuroimaging in neonatal hypoxic ischemic encephalopathy. Indian J Pediatr 83:995-1002.

Kurinczuk JJ, White-Koning M, Badawi N (2010) Epidemiology of neonatal encephalopathy and hypoxic-ischaemic encephalopathy. Early Hum Dev 86:329-338.

Leandrou S, Petroudi S, Kyriacou PA, Reyes-Aldasoro CC, Pattichis CS (2016) An overview of quantitative magnetic resonance imaging analysis studies in the assessment of Alzheimer's disease. In: XIV Mediterranean Conference on Medical and Biological Engineering and Computing 2016, p 281. Paphos, Cyprus: Springer.

Lemmon ME, Wagner MW, Bosemani T, Carson KA, Northington FJ, Huisman T, Poretti A (2017) Diffusion tensor imaging detects occult cerebellar injury in severe neonatal hypoxic-ischemic encephalopathy. Dev Neurosci 39:207-214.

Li HX, Feng X, Wang Q, Dong X, Yu M, Tu WJ (2017) Diffusion tensor imaging assesses white matter injury in neonates with hypoxic-ischemic encephalopathy. Neural Regen Res 12:603-609.

Liao H, Wang L, Zhou B, Tang J, Tan L, Zhu X, Yi J, Chen X, Tan C (2012) A resting-state functional magnetic resonance imaging study on the first-degree relatives of persons with schizophrenia. Brain Imaging Behav 6:397-403.

Liu HM, Chen XD, Hua XY (2012) Transplantation of human amniotic epithelial cells in treating neonatal rats with hypoxic-ischemic brain encephalopathy. Zhongguo Zuzhi Gongcheng Yanjiu 16:95-98.

Shi F, Yap PT, Wu G, Jia H, Gilmore JH, Lin W, Shen D (2011) Infant brain atlases from neonates to 1- and 2-year-olds. PLoS One 6:e18746.

Smyser CD, Snyder AZ, Shimony JS, Mitra A, Inder TE, Neil JJ (2016) Resting-state network complexity and magnitude are reduced in prematurely born infants. Cereb Cortex 26:322-333.

Striem-Amit E, Hertz U, Amedi A (2011) Extensive cochleotopic mapping of human auditory cortical fields obtained with phase-encoding FMRI. PLoS One 6:e17832.

Supekar K, Musen M, Menon V (2009) Development of large-scale functional brain networks in children. PLoS Biol 7:e1000157.

Vecchio F, Miraglia F, Romano A, Bramanti P, Rossini PM (2017) Small world brain network characteristics during EEG Holter recording of a stroke event. Clin Neurophysiol 128:1-3.

Wang JF, Chen HY, Li YX, Ye N, Feng L, Wang SN, Zhang YM (2017) Small-world networks analysis of leukoaralosis: a rest-state functional MRI study. Zhongguo Xingwei yu Nao Kexue Zazhi 26:977-982.

Watts DJ, Strogatz SH (1998) Collective dynamics of 'small-world' networks. Nature 393:440-442.

Yan CG, Cheung B, Kelly C, Colcombe S, Craddock RC, Di Martino A, Li Q, Zuo XN, Castellanos FX, Milham MP (2013) A comprehensive assessment of regional variation in the impact of head micromovements on functional connectomics. Neuroimage 76:183-201.

Zhang J, Zhang L, Xiang L, Shao Y, Wu G, Zhou X, Shen D, Wang Q (2017a) Brain atlas fusion from high-thickness diagnostic magnetic resonance images by learning-based super-resolution. Pattern Recognit 63:531-541.

Zhang L, Wang Q, Gao Y, Wu G, Shen D (2016) Automatic labeling of MR brain images by hierarchical learning of atlas forests. Med Phys 43:1175-1186.

Zhang L, Zhang H, Chen X, Wang Q, Yap PT, Shen D (2017b) Learning-based structurally-guided construction of resting-state functional correlation tensors. Magn Reson Imaging 43:110-121.

C-Editor: Zhao M; S-Editors: Yu J, Li CH; L-Editors: Qiu Y, Song LP; T-Editor: Liu XL